# A high-resolution, 3-D Model of Jupiter's Great Red Spot.

James Y-K. Cho,
Spectral Sciences Inc., 99 South Bedford Street, #7, Burlington, MA, 01803-5169

Manuel de la Torre Juárez,
M-S 238-600, JPL/Caltech, 4800 Oak Grove Dr., Pasadena, CA 91109-8099, USA.

Andrew P. Ingersoll,
Division of Geological and Planetary Sciences, California Institute of Technology,
Pasadena, CA 91125, USA.

David G. Dritschel.
Mathematical Institute, University of St. Andrews North Haugh, St Andrews KY 16 9SS, Scotland

Short title: HIGH RESOLUTION 3-D MODEL OF JUPITER'S GREAT RED SPOT

**Abstract.** The turbulent flow at the periphery of the Great Red Spot (GRS) contains many fine-scale filamentary structures while the more quiescent core – bounded by a narrow high-velocity ring – exhibits organized, possibly counter-rotating, motion. Past studies have neither been able to capture this complexity *nor* adequately study the effects of vertical stratification, $L_{\mathcal{R}}(z)$, on the GRS. We present results from a series of high-resolution, 3-D simulations which advect the dynamical tracer, potential vorticity. The detailed flow is successfully captured with a characteristic value of $L_{\mathcal{R}} \approx 2000$ km, independent of the precise vertical profile.

## Introduction

Voyager and Galileo's reconnaissance transformed our picture of the dynamical character of Jupiter's Great Red Spot (GRS). The high-resolution images returned by the spacecrafts revealed associated motions involving an enormous range of scales: the GRS is a coherent, synoptic scale ($\sim 10^4$ km) vortex rotating in a region of highly turbulent, fine-scale filamentary cloud structures (Fig. 1). The images also revealed that the most dynamic region of the vortex, defined by a steep velocity gradient, is concentrated in a very narrow band at its perimeter. Such strong, sharp gradients bounding a vortex are not unique in planetary atmospheres; for example, Earth's wintertime stratospheric polar vortices are also bounded by similarly steep gradients [*Juckes & McIntyre,* 1987]. For the Earth's atmospheric vortices, it has long been recognized that a crucial requirement in understanding the detailed flow structure is the ability of numerical models to resolve the fine-scales. In this report, we summarize the results from a series of high-resolution, 3-D numerical simulations of Jupiter's GRS and its environs; a well-tested method which advects the materially conserved tracer, potential vorticity (PV), is employed [*Dritschel & Ambaum,* 1997].

In the past, 2-D (1- or $1\frac{1}{2}$-layer) numerical simulations have been used, primarily focusing on the spot's dynamical origin and survivability [*Williams,* 1985; *Marcus,* 1988; *Dowling & Ingersoll,* 1989; *Cho & Polvani,* 1996]. These studies have shown that, despite their simplicity, single shallow-layer atmospheric dynamics models can successfully explain the longevity of the GRS under a variety of Jovian-like conditions. However, due to their limited horizontal resolution, those studies were unable to capture the detailed features of the complex flow observed within and around the GRS. In particular, in addition to the high-gradient band or ring feature previously mentioned, some of the features in Fig. 1 previously *not* captured are: 1) the strong southward

bending of the westward flow immediately to the north of the GRS; 2) the undulating filament trailing to the northeast of the GRS; 3) the fine-scale filamentary structures at the periphery of the vortex, which partially wrap around the GRS – giving its "cuspy" sides; and 4) the possibly organized, medium-scale ($\sim 1000$ km) structures at the core of the GRS. In addition, the full effects of atmospheric stratification, characterized by the Brunt-Väisälä (buoyancy) frequency, on the GRS was not studied since a high vertical resolution (many layers) is necessary for such a study. Only recently, two simulations with more than one vertical degree of freedom have been performed [*Achterberg & Ingersoll,* 1994; *Williams,* 1997]. However, they still lacked the horizontal resolution to capture the mentioned features of interest or to study the detailed effects of Brunt-Väisälä frequency on the flow in and around the GRS.

## Model

In this work, we model the region of the atmosphere in which the GRS can be followed with visible (cloud and haze) tracers. This region is stably stratified and rapidly rotating; hence, the motion is predominantly layer-wise. Therefore, we use the quasi-geostrophic (QG) approximation [*Pedlosky,* 1979], appropriate for any synoptic scale structure on timescales much shorter than the diabatic warming or radiative cooling times. The governing equation expresses the material conservation and transport of PV, $q$:

$$\frac{Dq}{Dt} \equiv (\frac{\partial}{\partial t} + \mathbf{v}\cdot\nabla)\, q = 0; \tag{1}$$

$$q = f + \nabla^2\psi + \frac{1}{\rho_0}\frac{\partial}{\partial z}(\rho_0 \frac{f_0^2}{N^2}\frac{\partial \psi}{\partial z}) + \Xi \tag{2}$$

In Eq. 1, $\mathbf{v}=(u,v) = (-\partial\psi/\partial y, \partial\psi/\partial x)$ is the horizontal velocity, where $\psi = \psi(x,y,z,t)$ is the streamfunction. In Eq. 2, $\nabla^2$ is the horizontal Laplacian; $f = f_0+\beta y$ is the Coriolis parameter, with $\beta$ the planetary vorticity gradient. $\Xi = \gamma(x,y,t)\delta(z)$ is the equivalent

sheet contribution to the PV by the generally inhomogeneous boundary condition [*Hoskins et al.*, 1985] at the bottom ($z=0$), with $D\gamma/Dt=0$ and $\delta(z)$ a Dirac delta function. $\rho_0(z)$ and $N(z)$ are the basic-state density and the Brunt Väisälä profiles, respectively, in log-pressure coordinate, $z$. The description and extensive tests of the numerical algorithm used to solve the governing equation are presented in Dritschel & Ambaum [1997].

## Results

The typical results from our numerical simulations are shown in Fig.'s 2 and 3. Although much of the computed detail far exceeds the resolution capacity of the graphics, the 3-D flow field is still quite complex. Therefore, the view from the top is presented for clarity, and the PV contours in the lower layers are shown in dashed lines. In all the simulations, the computational domain is doubly-periodic on the sides (of $2\pi\times10^4$ km each) with a flat bottom ($\partial\psi/\partial z = 0$, $\gamma = 0$) and a free surface ($\partial\psi/\partial z + N^2\psi/g = 0$) at the top ($z = 1.25H_s$, where $H_s$ is the density scale height). The latter boundary condition is general and reduces to the traditional "rigid-lid" approximation ($\partial\psi/\partial z \to 0$) for a weakly stratified atmosphere ($N \to 0$).

In Fig. 2, a *8-layer* (8 vertical modes) simulation is shown at two different times; we have performed calculations with up to 60-layers and have verified that the results presented here do not change qualitatively with higher vertical resolution. Here, $N(z) = N^*z$, where $N^* = cN_s$ with $c =$ constant and $N_s \equiv (g^2/T_sc_p)^{1/2} = 0.017$ 1/s, using the standard Jupiter values [*Ingersoll*, 1990] of $g=22.9$ m/s$^2$, $c_p=13213$ m$^2$/s$^2$K, and $T_s = 140$ K. The density scale height, $H_s \equiv RT_s/g$, is 23.1 km with $R = 3779.1$ m$^2$/s$^2$K; the *characteristic* Rossby deformation radius, $L_{\mathcal{R}}^* \equiv N^*H_s/f_0$, is 2000 km with $f_0 = 4\pi\sin(-22.5)/35740$ 1/s $= 1.3\times10^{-4}$ 1/s; and, the relative density and

pressure profiles are $\rho(z)/\rho(0) = p(z)/p(0) = \exp(-z/H_s)$. The simulation time unit, $t = 1$, corresponds to 0.2 Jovian days, or approximately 0.1 GRS turnaround times; a fourth-order accurate Runge-Kutta scheme is used for the timestepping.

The common initial configuration for all the cases discussed in this work is shown in Fig. 2a. In the domain, uniform areas of PV are contoured by lines, which are advected by the flow. Thus, the lines serve as flow tracers. The GRS is initially specified as an elliptical column of uniform relative vorticity $(q - f)$, centered at $-22.5°$ with semi-major and semi-minor diameters of $2 \times 10^4$ km and $1 \times 10^4$ km, respectively. The column is "embedded"[1] in a pair of barotropic ($z$-independent) E-W jets: one westward at $-20°$ latitude and the other eastward at $-28°$ latitude. A jet here is comprised of two uniform strips of PV, with each strip representing an edge (equatorward or poleward) of the jet and the jump between them corresponding to the jet core (extremum); the size and strength of a jet is related to the width of the strips and the jump value between them. In our simulations, a series of strips and jumps are chosen to initially match the zonal (E-W) jets observed by Limaye [1986] at the latitudes near the GRS. The resulting flow is due to the individual contributions from the vortex, the jets, and the planetary rotation. The situation is similar to that in several past simulations. However, unlike in those studies, the jets in our study more accurately represent the observed flow near the GRS, deflecting from their respective latitudes and bending around the vortex column as they zonally traverse the domain[2]. Note also that the dynamical structures in our simulations (vortex and jets) interact and evolve freely, without being subject to the influence of externally imposed conditions (e.g., uniform shear or bottom topography);

---

[1]In the observations, as well as in our simulations, the GRS "overfills" the jets.

[2]See, for example, the line immediately north of the ellipse, which span E-W all the way across the domain.

the evolution, including any baroclinicity that develop, is strictly due to the nonlinear interaction between the free structures in the flow. The important effects of imposed, *dynamic* (i.e., time-dependent) bottom boundary conditions, arising from the neutrally stable motion from below, will be reported elsewhere.

Starting with the initial condition depicted in Fig. 2a, the evolution after 533 time units (~53 GRS rotations) is shown in Fig. 2b. By comparing Fig. 2b with Fig. 1, it can be seen that numerous detailed features in the latter, *not* obtained in previous simulations, are realistically captured in this simulation. First, thin filaments are formed and advected around the elliptical vortex column, tracing a cuspy, "cat's eye" flow pattern, which resembles very closely the actual flow around the GRS. Second, the initial E-W symmetry of the flow is clearly broken as the westward flow north of the GRS is substantially pulled southward at the northwestern side of the vortex. Third, a tight ring of high PV gradient (bundle of PV lines) is formed, capturing the familiar, characteristic "collar" of the GRS. In both the simulation and in observations, the ring corresponds to a well-organized circulating region of high velocity in the flow. In QG dynamics, such a sharp feature is a natural consequence of a small $L_{\mathcal{R}}$(small compared to the size of the vortex); here, $L_{\mathcal{R}}$varies linearly from 0 km at the bottom to 2000 km at the top. Another consequence is the relatively quiescent (compared to the ring) vortex center, where there is a notable absence of comparably large-scale, organized structure; instead, the center contains smaller-scale ($\sim 1000$ km) coherent structures, which slowly counter-rotate with respect to the outer ring (Fig. 2b). We also note here some baroclinicity ($\partial \mathbf{v}/\partial z$) in the flow – exhibited by the dashed lines – due to the strong stratification; but, the flow is, in general, barotropic (vertically coherent), as in the Voyager and Galileo observations. A longer time integration (of up to $t = 2000$) shows the vortex to be stable and the overall flow to be not too different from that in

Fig. 2b, except for a westward translation due to drift caused by the $\beta$-effect.

For an atmosphere in hydrostatic equilibrium, with vertical temperature profile $T = T(z)$ and lapse rate $\partial T/\partial z$, the buoyancy frequency profile, $N(z) = [\ g(\partial T/\partial z + g/c_p)\ /\ T\ ]^{1/2}$. The $N(z) = N_s\phi(z)$ profile used in the simulation of Fig. 2(b), where $\phi(z)$ is an arbitrary function, is based on the temperature profiles obtained by the Voyager radio occultation measurements [*Lindal et al.* 1981] and is similar to a previously used profile [*Achterberg & Ingersoll* 1989]. Note that the uncertain moisture content of Jupiter's atmosphere most strongly affects the stability structure far below the visible cloud deck and, given our results, is not expected to play a significant, stabilizing dynamical role. That is, in our simulations we have observed that the evolution is not critically sensitive to the precise functional form (e.g., linear, quadratic, exponential, or even constant) of the $N(z)$ profile in the modeled height range. It is, however, very strongly sensitive to the maximum value of $N(z)$, clearly establishing the dynamically significant role of $N^*$ (hence, $L_R^*$) for the GRS and its surrounding region on Jupiter.

The role of $L_R$ in geophysical-astrophysical fluid dynamics is well known. Of particular interest here is its ability to screen and reduce the interaction strength between the flow structures. The GRS and the background jets are shielded from their mutual interaction approximately exponentially fast with their separation distance. In addition, it has been recently shown that a QG vortex column of height-to-width ratio, $\delta$, less than roughly $3f_0/N = 3H_s/L_R$ (here, $\delta \sim 0.001$ and $3f_0/N \sim 0.01$) in a horizontal straining field is baroclinically stable to 3-D disturbances [*Dritschel & de la Torre Juárez,* 1996]. That is, a *weakly-interacting, coherent* shallow vortex column is both horizontally and vertical stable: hence the localized, coherent, and predominantly barotropic look of the flow in Fig. 2b – and, we believe, the GRS. To illustrate this point

further, the dynamical responses to variations in $N^*$ are shown in Fig. 3.

Fig. 3a shows the behavior for a case with all simulation parameters identical to those of Fig. 2b, except with $N^* \rightarrow 2N^*$. The characteristic Rossby deformation radius, $L_{\mathcal{R}}^*$, is now 4000 km. The flow is shown at $t=360$, or $\sim$36 GRS rotations. Initially, the evolution for this case is similar to that in Fig. 2b. However, due to the increase in the interaction length, the vortex is no longer weakly interacting; and, the evolution is much more dynamic in this case. After a brief "similar" period (at $t \sim 250$), the jet-vortex system quickly and violently becomes unstable, as shown in Fig. 3a. Most notably, the vortex begins to precess and eventually splits the bottom eastward jet, deflecting part of it southward on the west side of the GRS and northward on the east side. Afterwards, the two deflected streams suffer Kelvin-Helmholtz instability (large undulations of the PV due to adverse horizontal shear, $\partial q/\partial y$), and vertical sheets of PV roll up into many vortex columns south of the GRS. This is contrary to observations. In addition, unlike in the previous case, the core always co-rotates with the outer ring; hence, no counter-rotating motion is observed in this case. The only common feature with the previous case is that the evolution is again quite barotropic, even after a long time; only in the passive (weak), thin filaments are there signs of baroclinicity.

Fig. 3b shows the behavior for a case with all simulation parameters identical to those of Fig. 2b, except with $N^* \rightarrow N^*/2$. Therefore, $L_{\mathcal{R}}^*$ is now 1000 km. The flow is shown at $t=3300$, or $\sim$330 GRS rotations. As in Fig. 3a, the flow is again markedly different than that shown in Fig. 2b. In this case, the vortex is *not* coherent. There is an immediate and severe vortex wave breaking in the northwestern sector of the vortex; and, weak trailing vortices and tangles of filaments form later east of the vortex. Most notably, the PV in the latitude band in which the vortex was initially located eventually becomes very well-homogenized – to the point that the "GRS" is now even difficult to

detect (Fig. 3b). This means none of the characteristic features of the GRS, such as the ring, is present. As discussed earlier, this loss of coherence is due to the small interaction length, $L_{\mathcal{R}}$; as a consequence, the vortex cannot maintain its shape as it effectively loses the ability "feel" the other side of itself. In addition, for a long time ($\sim$1000 time units), there is no core motion at all. These behaviors are all again contrary to observations. As expected, we have observed that the loss of coherence is even more pronounced in the cases with smaller $N^*$, in which the "GRS" completely fails to maintain its oval shape and is simply smeared out into a band. Although, both of the behaviors in Fig. 3 are permissible solutions of the QG equation, they are *not* observed on Jupiter. Hence, the most likely $N(z)$ profile for the GRS is the one used in the case of Fig. 2b.

## Summary

In conclusion, followingMarcus [1988] andAchterberg & Ingersoll [1994], we have used QG dynamics to model Jupiter's GRS. Here, we have extended the previous studies by performing our simulations with unconstrained structures *and* with much greater horizontal and vertical resolutions. Since the actual vertical structure of the atmosphere ($L_{\mathcal{R}}(z)$) at the GRS region is not known, we have assumed several representative structure profiles and found that, the 3-D flow is very sensitive to the characteristic value of the deformation radius, $L_{\mathcal{R}}^*$ (while less sensitive to the precise functional dependence on $z$): the case with $L_{\mathcal{R}}^* \approx 2000$ km gives realistic-looking flows while the cases with $\approx$4000 km and $\approx$1000 km do not. The 2000 km value is consistent with the vertical structure profile obtained byLindal et al. [1981] for several locations on Jupiter away from the GRS region, suggesting that that profile may be more representative of the entire planet. Our simulations show that, although physically simple, the QG model can capture very accurately the highly complex flow patterns revealed in Voyager

and Galileo images, as well as tightly constrain and identify the crucial aspects of the vertical structure of the region in and around the GRS.

**Acknowledgments.** J.Y-K.C. and A.P.I. were supported by the NASA's Planetary Atmospheres Program; M.T.J. was supported by NASA/N.R.C.; and, D.G.D. was supported by N.E.R.C. J.Y-K.C. and M.T.J. thank Ashwin Vasavada and Adam Showman for helpful discussions.

## References


Achterberg, R. K. and A. P. Ingersoll, A normal-mode approach to jovian atmospheric dynamics. *J. Atmos. Sci.* **46**, 2448–2462, 1989.

Achterberg, R. K. and A. P. Ingersoll, Numerical simulation of baroclinic Jovian Vortices. *J. Atmos. Sci.* **51**, 541–562, 1994.

Cho, J. Y-K. and L. M. Polvani, The morphogenesis of bands and zonal winds in the atmospheres of the giant outer planets. *Science* **273** 335–337, 1996.

Dowling, T. E. and A. P. Ingersoll, Jupiters Great Red Spot as a shallow-water system. *J. Atmos. Sci.* **46** 3256–3278, 1989

Dritschel, D. G. and M. de la Torre Juárez, The instability and breakdown of tall columnar vortices in a quasi-geostrophic fluid. *J. Fluid Mech.* **328**, 129–160, 1996.

Dritschel, D. G. and M. H. P. Ambaum, A contour-advective semi-Lagrangian algorithm for the simulation of fine-scale conservative fields. *Q. J. Roy. Meteorol. Soc.* **123**, 1097–1130, 1997.

Hoskins, B. J., M. E. McIntyre, and A. W. Robertson, On the use and significance of isentropic potential-vorticity maps. *Q. J. Roy. Meteorol. Soc.* **111**, 877–946, 1985.

Ingersoll, A. P. Atmospheric Dynamics of the outer planets. *Science* **248**, 308–315, 1990.

Juckes, M. N. and M. E. McIntyre, A high resolution, one-layer model of breaking planetary waves in the stratosphere. *Nature* **328**, 590–596, 1987.

Limaye, S. S. Jupiter: New estimates of the mean zonal flow at the cloud level. *Icarus* **65**, 335–352, 1986.

Lindal, G. . G. E. Wood, G. S. Levy, J. D. Anderson, D. N. Sweetnam, H. B. Holtz, B. J. Buckles, D. P. Holmes, P. E. Doms, V. R. Eshleman, G. L. Tyler, T. A. Croft, The atmosphere of Jupiter: An analysis of the Voyager radio occultation measurements. *J. Geophys. Res.* **86**, 8721–8727, 1981.

**Figure 1.** Jupiter's Great Red Spot(GRS): a mosaic from Voyager, with orientation as indicated. The GRS is characterized by: 1) a high-velocity ring feature demarcating its boundary; 2) a strong southward bending of westward flow at the northwestern side; 3) trailing undulations to the northeast; and, 4) the fine-scale filamentary structures at the periphery of the vortex

**Figure 2.** Potential vorticity iso-contours from a 8-layer simulation with $N(z) = N^* z$ such that $L_{\mathcal{R}}^* \approx 2000$ km: a) $t = 0$, and b) $t = 533$, where $t = 1$ corresponds to approximately 0.1 GRS turnaround times. The field is a superposition of the individual vorticity contributions from the vortex, the jets, and the planetary rotation. The material lines, which demarcate areas of constant potential vorticity, are colored in order to aid in identifying the initial position of the spot and jets; as with all material lines, they subsequently move with the flow. The top view is shown. The flow in b), which evolved starting from the configuration in a), very realistically resembles the observation (compare with Fig. 1): the shape, stability, fine-scale filamentary structures, as well as the core motion, are all captured in this simulation. There is no qualitative difference in the flow pattern at $t = 2000$ or with 60-layer vertical resolution.

**Figure 3.** Potential vorticity iso-contours from two different simulations with all parameters identical to those of Fig. 2, except $N^*$: a) *twice* and b) *half* of that in Fig. 2b, respectively. The flow fields at $t = 360$ in a) and $t = 3300$ in b) are shown; the initial configurations for both simulations are as in Fig. 2a. The $N^*$ (hence $L_{\mathcal{R}}^*$) values in both simulations lead to unstable or incoherent GRS, in direct contrast to the observations; thus, they are not the appropriate values for the GRS.

Marcus, P. S. Numerical-simulation of Jupiters Great Red Spot. *Nature* **331**, 693–696, 1988

Pedlosky, J. *Geophysical Fluid Dynamics*, Second Ed., Springer, New York, 1979.

Williams, G. P. Jovian and comparative atmospheric modeling. *Adv. Geophys.* **28A**, 381–428, 1985

Williams, G. P. Planetary vortices and Jupiter's vertical structure. *J. Geophys. Rev.* **102**, 9303–9308, 1997.

---

James Y-K. Cho, Spectral Sciences Inc.; 99 South Bedford Street, #7, Burlington, MA, 01803-5169, (e-mail: jcho@spectral.com)

Manuel de la Torre Juárez, M-S 238-600, JPL/Caltech, 4800 Oak Grove Dr., Pasadena, CA 91109 (e-mail: mtj@cobra.jpl.nasa.gov)

Andrew P. Ingersoll, Division of Geological and Planetary Sciences, California Institute of Technology, Pasadena, CA 91125, USA (e-mail: api@gps.caltech.edu)

David G. Dritschel, Mathematical Institute, University of St. Andrews North Haugh, St Andrews KY 16 9SS, Scotland (e-mail: dgd@st-and.ac.uk)

Received April 20, 2000; revised April 20, 2000; accepted April 20, 2000.

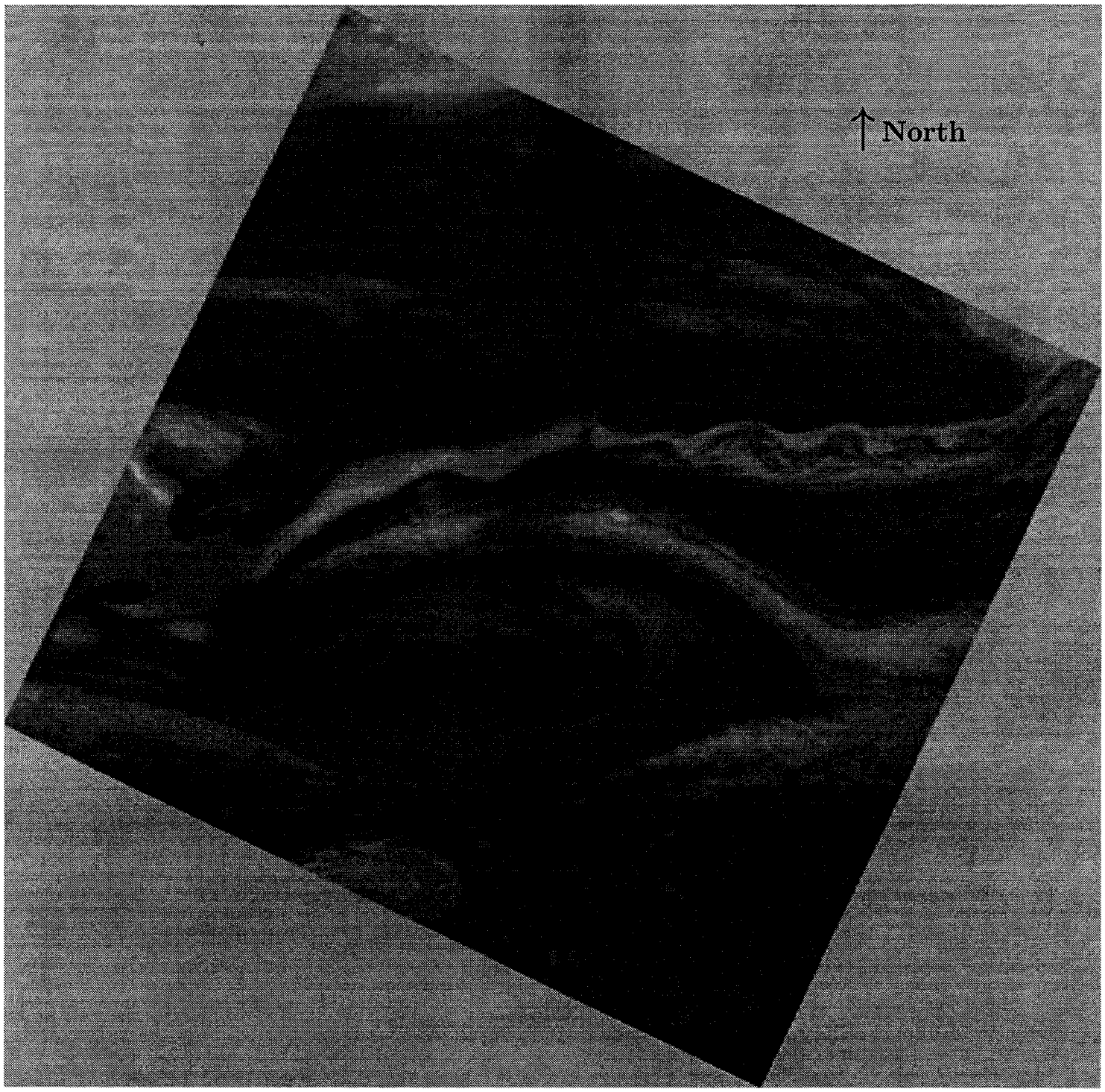


# Figure 1

J. Y-K Cho et al: *A High-Resolution, 3D Model of Jupiter's Great Red Spot.*

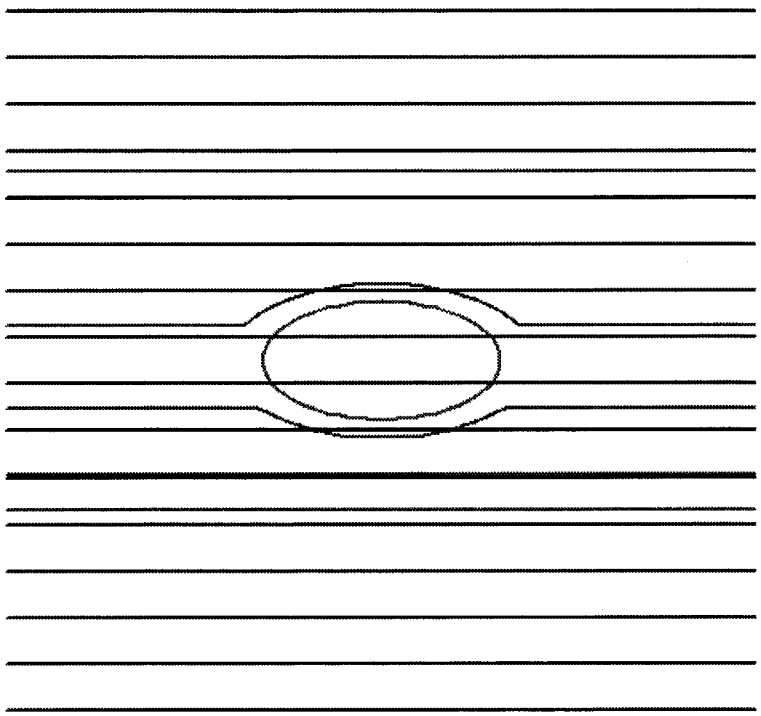

Figure 2a

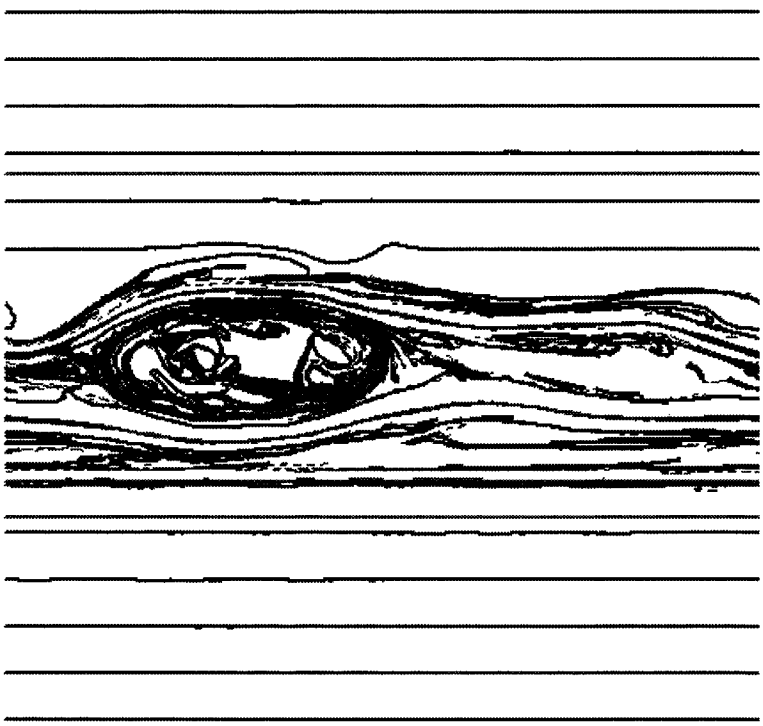

Figure 2b

Figure 3a

Figure 3b

**J. Y-K Cho et al.** *A High-Resolution, 3D Model of Jupiter's Great Red Spot.*